Development and calibration of a microfluidic biofilm growth cell with flow-templating and multi-modal characterization

François Paquet-Mercier, Adnane Kara§, Muhammad Safdar[a], Nahid Babaei Aznaveh, Mirpouyan Zarabadi, Jesse Greener*

***Abstract*—We report the development of a microfluidic flow-templating platform with multi-modal characterization for studies of biofilms and their precursor materials. A key feature is a special three inlet flow-template compartment, which confines and controls the location of biofilm growth against a template wall. Characterization compartments include Raman imaging to study the localization of the nutrient solutions, optical microscopy to quantify biofilm biomass and localization, and cyclic voltammetry for flow velocity measurements. Each compartment is tested and then utilized to make preliminary measurements.**

I. Introduction

Biofilms are comprised of colonies of microorganisms within a protective extracellular polymeric matrix. Therefore, biofilms are robust, making them important systems of study in medicine, due to their potential for pathogenesis and their resistance against anti-microbial drugs [1]. We are particularly interested in the potential of biofilms as new engineered biomaterials for the catalysis of important biochemical reactions, e.g., for the synthesis of fine chemicals and even energy generation [2,3]. The key to achieving this goal lays in the ability to better control and measure biofilm properties [4,5].

We seek to control biofilms by exploiting the relationship between the hydrodynamic environment and the final biofilm properties [6]. Microfluidics is an ideal technology for this purpose because liquids flow with very low Reynolds numbers, resulting in highly controllable laminar flow and shear forces. New manuscripts have been published which use microfluidic channels to study the effect of well-defined shear forces on biofilm properties (physical morphology, mechanical properties), their behaviour in dynamic environments (growth rates, adsorption/detachment, streamer formation, planktonic cell proliferation) and their interaction with anti-fouling surfaces [7-19].

Research supported by (i) Fonds de recherche du Québec – Nature et technologies (FRQNT) and (ii) Princeton Research-Gamble Technologies.

All authors are with Département de Chimie, Université Laval, 1045 Avenue de la Médecine, Québec, QC G1V 0A6, Canada.

[a] Author M.S. has co-affiliation: Department of Chemistry, University of Eastern Finland, Yliopistokatu 7, FI-80101 Joensuu, Finland.

§Co-first author.

* Correspondence should be sent to J.G. via phone: (418) 656- 2131 x7157 or email: jesse.greener@chm.ulaval.ca)

An ongoing problem in the studies of biofilms in rectangular microchannels is that the hydrodynamic shear stress is much lower in the corners than elsewhere. This results in biofilms with strong variations in thickness and related properties. Uncontrolled growth in microchannels can also result in overgrowth, which can strongly impact the local hydrodynamic environment [18,19]. To rectify this problem, our group has developed a flow-templating micro-bioreactor (FT-μBR), which confines biofilms to specific locations within the channel. The resulting biofilms are more homogenous and are better subjects for quantitative analytic studies [15]. However, the impact of patterned biofilms on the hydrodynamic environment remains to be studied.

In order to address the mismatch between the enhanced control over biofilm growth conditions in the FT-μBR and the limited options for *in situ* characterization, the focus is presently the integration of multiple characterization modalities into the FT-μBR. We have chosen three modes for the integration into the FT-μBR based on their availability, cost, and their utility in biofilm studies. These include, optical density measurements, which have been shown to be directly related to the biomass *via* the Beer-Lambert law [20]; Raman spectroscopy, which is a versatile tool that can be used to report on the chemistry of biofilms, the surrounding liquid environments and even the solution temperature, without the need for material preparation or the addition of external probe species [21]; and cyclic voltammetry (CV), which can rapidly generate votammograms detailing biofilm biochemical activity, solution phase concentrations and local flow velocities [22,23]. Therefore, in this paper we discuss the developments toward a bioreactor, which includes four functional compartments for: (i) flow-templating biofilm growth, (ii) optical density measurements *via* optical microscopy, (iii) surface enhanced Raman spectroscopy (SERS) for measurements of chemical concentrations in the biofilm growth zones, and (iv) multipoint CV measurement for measurements of liquid flow velocities to determine the impact of the biofilm on the hydrodynamic environment in the microchannel.

II. Experimental

Syringe pumps (PHD 2000, Harvard Apparatus, Holliston, MA, USA) were used to supply liquids to the FT-μBR. Perfluoroalkoxy (PFA) fluidic tubing with outer diameter 1.6 mm (U-1148, IDEX, WA, USA), was connected to 60mL

syringes (BD Scientific, NJ, USA) *via* connectors (P-200x, P-658, IDEX, WA, USA). Aqueous solutions were formed from sodium citrate (Sigma Aldrich) and ultrapure water (resistivity of 18.1 MΩ·cm). Microfluidic device fabrication materials also included polydimethyl siloxane (PDMS) (sylgard184, Dow corning, Canada) and indium tin oxide coated glass cover slips (8-12 Ω/sq., Diamond Coatings, Halesowen, UK). The cyclic voltammetry compartment included gold coated pins (609-3210-ND, DigiKey Corporation, Canada). Air plasma treatments were used for PDMS to PDMS and PDMS to glass bonding and nanostructuring of the silver surface were performed at 600 mTorr using a plasma cleaner (PCD-001, Harrick Plasma, Ithaca, NY, USA). Nutrient solution was a modified AB media consisting of 1.51 mM $(NH_4)_2SO_4$, 3.37 mM Na_2PO_4, 2.20 mMKH_2PO_4, 179 mM NaCl, 0.1 mM $MgCl_2$, $CaCl_2{\cdot}2H_2O$, 0.001 mM $FeCl_3$ and 10 mM sodium citrate (Sigma Aldrich). *Pseudomonas sp.* strain CTO7 was used for the biofilm formation. The bacterial culturing procedures are described elsewhere [15]. Optical microscope measurements were conducted using microscope stage (BX30, Olympus) attached to a confocal Raman spectrometer (LABRAM 800HR, Horiba Jobin Yvon, Villeneuve d'Ascq, France) or using a standalone inverted microscope (IX73, Bruker) in bright-field, reflection and epifluorescence modes. Images were collected using an uncooled, monochrome CCD camera (Lumenera Infinity 3-1, Ottawa, Canada). Optical measurements were conducted on solutions containing dyes (McCormick, London, Canada). SERS measurements were conducted using the same confocal Raman system as above, with 100x objective. The excitation source was an Ar^+ laser setted at 514,5 nm (Coherent, INOVA 70C Series Ion Laser, Santa Clara, CA, USA). Chemicals used for electroless deposition and electro roughening included chloroauric acid, glucose, potassium bicarbonate, silver nitrate, L-tartaric acid and ammonium hydroxide (Sigma Aldrich). Atomic force microscopy (AFM) measurements were performed in tapping mode at ambient conditions (Nanoscope III Multimode, Digital Instruments, Santa Barbara, CA, USA) with NSC15\AlBS silicon standard probes (Mikromasch, Lady's Island, SC, USA). UV-Vis spectra of the metal surfaces were recorded in diffuse reflectance mode using a Praying Mantis accessory (Harrick Scientific, Pleasantville, NY, USA) on a Cary 500 Scan spectrophotometer (Varian, Palo Alto, CA, USA). Electrochemical measurements were conducted using research grade potentiostat (Versastat 4-500, Princeton Applied Research). For automated sequential measurements of 6 working electrodes *via* CV, the potentiostat was interfaced with a home-built 8-channel analog multiplexer (568-1689-5-ND IC MUX/DEMUX 8X1 16DIP, DigiKey, Canada). The potentiostat software (VersaStudio v2.20) selected the multiplexer channel *via* selection of TTL output which served as control bits. CV measurements of biofilm precursor materials were conducted by adding a known amount of potassium ferricyanide (244023, Sigma Aldrich, Canada) and supporting electrolyte solution 0.5 M KNO_3 and 0.5 M KOH to the biofilm nutrient solution. All voltammograms were obtained in the potential window in which water dissociation reactions such as hydrogen and oxygen evolution are not involved.

III. System Setup And Calibration

A. Overall system architecture

Fig. 1A shows the schematic of the proposed platform, which consists of 4 compartments. The flow templating compartment isolates the nutrient solution into linear patterns against the templating wall of the microchannel. It is a triple inlet system consisting of Inlet 1 confinement flow, Inlet 2 and 3 for the formation of up to two separate template-flows of nutrient and inoculant solutions, respectively. Flow rates through these inlets are referred to as Q_C, Q_{TN}, Q_{TI}, respectively, with $Q_{TOT} = Q_C + Q_{TN} + Q_{TI}$. The channel width was w=2mm, h=305µm, l=12mm. The benefit of the three inlet system is that adsorbed bacteria in the inoculant channel will not consume citrate growth solution before it flows into the measurement channel. The second compartment is for optical characterization of biofilm optical density and its precursor materials. This compartment is either completely transparent for imaging in bright-field or reflection mode imaging can be conducted from reflective metal surfaces. The third compartment features a nanostructured metal surface at the biofilm templating wall.

A

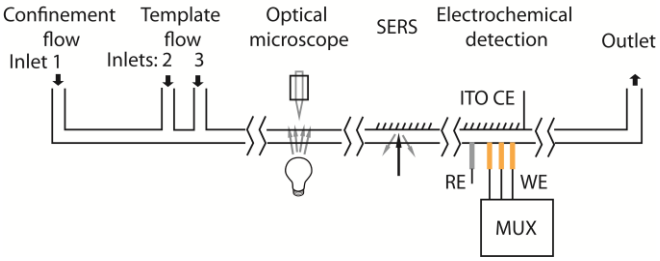

B

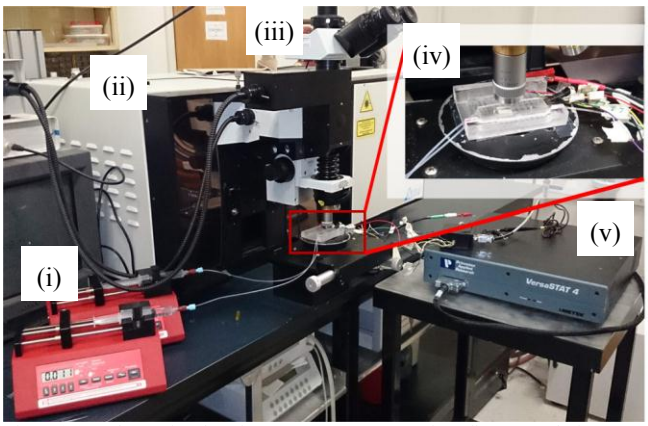

Fig. 1(A) Schematic showing 4 compartments for: flow-templating, optical characterization, SERS and electrochemical detection. In the electrochemical compartment, a voltage is applied between a transparent ITO counter electrode (CE) and up to 6 separate working electrodes (WE) relative to a reference electrode (RE). Each WE is accessed individually by a multiplexer (MUX). (B) An image showing the microfluidic device interfaced with the microscope stage of the Raman spectrometer, capable of both optical and Raman measurements, and a potentiostat for cyclic voltammetry measurements. Highlighted are syringe pumps (i), Raman spectrometer (ii), optical microscope stage (iii), microfluidic device with fluidic and electrical connections (iv), and a potentiostat (v).

The plasmonic frequency is tuned by manipulating the size of the nanostructures to match the excitation laser frequency for SERS measurements. The final compartment consists of multiple working electrodes (WE) that enable site specific electrochemical measurements, an indium tin oxide counter electrode (ITO CE) and a gold reference electrode (RE). Fig. 1B shows a photograph of the complete prototype setup. The following sections describe the development and measurements acquired from individual compartments.

B. Flow Templating Compartment

Typically, biofilm growth in microchannels is uncontrolled. This can present a problem, because there are significant differences in flow velocities flowing through the corners of rectangular microchannels, compared to the other regions (Fig. 2A). The relation between the flow velocity, v ($m \cdot s^{-1}$), and the local shear force, τ (Pa), which is a primary factor in biofilm growth is given by:

$$\tau = \Delta v / d \cdot \mu \qquad (1)$$

where $\Delta v = v_w - v_c$ (the velocity at the wall and in the center of the channel, respectively), d (m) is the distance between the two local velocities that define Δv and μ (Pa·s) is the kinematic viscosity. The no slip condition imposed on pressure and volumetric driven fluid flow in a microchannel results in velocity at walls to be zero. Therefore, (1) can be rewritten as with $\Delta v = v_c$.

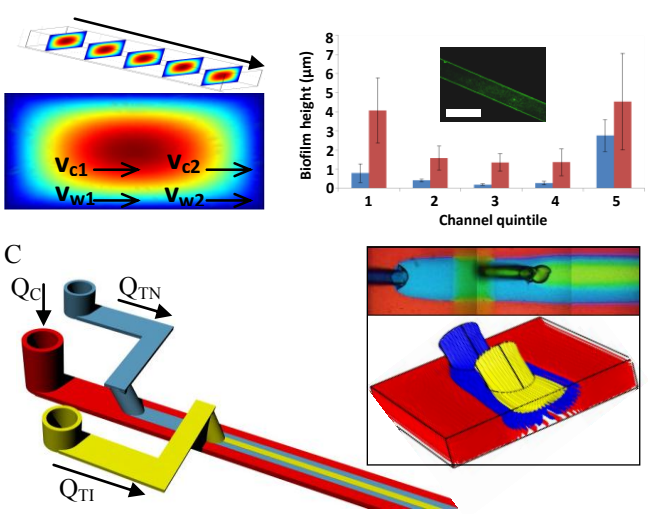

Fig. 2(A) computer simulation showing a series of cross-sections of the flow velocity in a simple rectangular channel. The arrow shows the direction of flow. Red indicates fast fluid velocity and blue is slow. A close-up is also shown for one cross-section with local velocity markers at 4 different positions (v_{w1} at the wall near the middle of the channel, v_{w2} is at the wall near the channel corner; v_{c1} is a distance d from the position of v_{w1}; and v_{c2} is a distance d from the position of v_{w1}). (B) Results from confocal laser scanning microscopy showing the pronouncement of growth in the corners after 24 h (blue) and 48 h (red). Error bars were from the standard deviation from 5 different height measurements conducted in the same quintile. Inset: Epifluorescence image of a rectangular channel (width 2 mm, height 200 µm) with biofilm culture 24 h after uncontrolled inoculation. (C) Cartoon showing the three inlet system with confinement flow (red, with flow rate Q_C) nutrient template flow (blue, with flow rate Q_{TN}) and inoculant template flow (yellow, with flow rate Q_{TI}). Upper inset shows a colour micrograph of the system with red, blue and yellow dye laden streams each flowing at 0.1 $mL \cdot h^{-1}$. Bottom inset shows a 3D flow simulation with segregated co-flowing template streams (blue and yellow) against the template wall (top).

We note that regions of low shear stresses can result in thick biofilms (Fig. 2B). We use flow templating to prevent the accumulation of biofilm in the corners. This is accomplished by forming a templating stream, which is localized in the channel by a confinement flow consisting of a biofilm growth inhibiting solution [15]. The width and height of the nutrient or inoculant template streams can be controlled by the flow rate ratio between the template and confinement streams, i.e. either Q_{TI}/Q_C or Q_{TN}/Q_C, respectively.

C. Optical Characterization Compartment

Using optical microscopy in transmission, reflection or dark-field modes, the template stream can be imaged. Fig. 3A shows a dye-laden template solution with a clear confinement stream flowing at the sides and above the template stream. We determined the pixel intensity along the channel cross-section, which was low for the light absorbing template stream, and high for the confinement stream (Fig. 3B). Using the Beer-Lambert relation we could calculate the corresponding height of each pixel by assuming that the light absorbance is due solely to the change in the path length through the absorbing medium, not a change in the local concentration of the template solution. This is reasonable, since the laminar flow environment of the microchannel results in the suppression of mass-transfer by convection and diffusion-based mass transfer out of the template stream is negligible during liquid residence times (30 s maximum). The resulting height profile based on this transformation shows that biofilm growth will be confined in three-dimensions by the template solution (Fig. 3B).

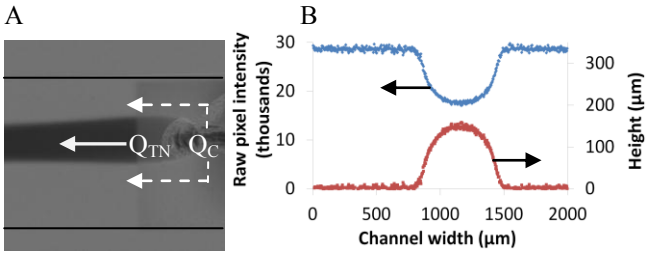

Fig. 3(A) Visualization of dye containing template flow from one junction in the FT-µBR using flow rates Q_C = 2.0$mL \cdot h^{-1}$ (dashed arrows) and Q_{TN} = 0.55$mL \cdot h^{-1}$ (solid arrow) in a channel with width 2000 µm and height of 305 µm. (B) Quantified optical data along a cross-section of (A), consisting raw pixel intensity (blue) and calculated height profile (red).

D. SERS Characterization Compartment

In the next step, we introduced a metallic layer at the bottom of the microchannel. The metal silver and gold layers were formed by electroless deposition, which allowed deposition on the non-conductive PDMS surface [24,25]. We could control the deposition location, thereby enabling site-selective SERS measurements. We then transformed the metal surface into a plasmonic surface capable of supporting SERS. For silver, this was accomplished via exposure to plasma gases, which resulted in the appearance of a

plasmonic absorption band near 400 nm (Fig. 4A). The origin of this effect is from the nanostructuring of the surface of the metal layer (Fig 4C,D). The addition of a silver SERS surface had two important effects: (i) enhancement of the Raman sensitivity by 4 orders of magnitude relative to regular Raman (with no SERS effect) and (ii) the masking of interfering signal from the polymer surface of the microfluidic wall. Full details of the process for depositing and generation of a SERS surface is given elsewhere [17]. We also investigated the use of gold as a SERS surface material in order to avoid possible anti-microbial effect of silver on the biofilm and to have a highly stable metal surface that can withstand high salt concentrations and redox side reactions in the presence of biofilm microbes' redox-based metabolism. We note, that the *Pseudomonas sp*. biofilms in this study showed no negative effects of growing on silver SERS surfaces. In this approach, we utilized electro roughening approach to transform the gold surface into a SERS surface with plasmonic absorbance band between 550 and 600 nm (Fig. 4B). We prepared nanostructured gold surfaces by electrodeposition from a 5 mM $HAuCl_4$ solution at pH 4 while holding the potential at 0.539V *vs* Ag/AgCl (NaCl 3.0M) [26]. Sodium citrate concentrations at the of the metal surface can be determined by SERS that uses a calibration technique that determines the ratio between the νC-COO band from sodium citrate (952 cm^{-1}) and the νO-H band of water (3435 cm^{-1}) [17].

E. Electrochemical Characterization Compartment

Electrochemical tools hold great potential to give wide range of information, *in situ*. Cyclic voltammetry, in particular, is a quantitative tool with wide applications due to its fast scanning (up to 10 $V \cdot s^{-1}$), ability to discriminate between analytes and to report on concentrations. We are interested in

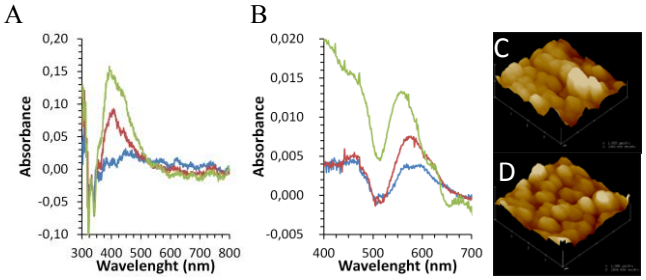

Fig. 4(A) Changes in plasmonic band for nanostructured silver surface with time of exposure to air (0.5, 7 and 16 minutes in blue, red and green, respectively). (B) Change in plasmonic band for nanostructured gold surface with time of electrochemical treatment (1, 2 and 10 minutes, in blue, red and green, respectively). (C) AFM image of silver surface before exposure to air plasma and (D) the same surface after exposure to air plasma (600 mTorr at 29.6 W for 16 minutes).

the technique due to its ability to measure biofilm redox activity and its sensitivity to flow velocities in microchannels [22,23]. In this work we integrate 6 working electrodes into the channel, with the eventual goal of directly studying biofilm properties at different locations. In the current application, however, we use CV measurements to measure deviations in the flow velocity to monitor flow redistribution around biofilms in response to their growth.

The working electrodes were mini rectangular gold coated pins with cross-sectional dimensions 120 x 380 µm. Each pin was connected to a homebuilt multiplexer, which was controlled by the potentiostat software. We used a gold pin as a pseudo reference electrode. The potential of the quasi-reference electrode was found to be 147 mV vs Ag/AgCl and it was stable during the experiments. The counter electrode was an ITO layer attached to the inside of the glass coverslip, which was used to seal the device. We undertook a series of calibration experiments designed to demonstrate the functionality of the CV compartment. The chosen analyte for the calibration measurements was potassium ferricyanide.

First, we demonstrated that data acquisition within the microfluidic environment works the same as for off-chip experiments (conducted in bulk solutions). Fig. 5A shows the cyclic voltammogram from a 6 mM aqueous potassium ferricyanide ($K_3Fe(CN)_6$) solution taken off-chip and in the microchannel using the exact same electrode configuration. The off-chip electrochemical cell showed a higher overall current than did the microfluidic experiments, likely due to larger contact area between the working electrode and the solution. Importantly, however, the shape and the position of the redox peaks, were nearly the same in each case. A quasi-reversible redox behaviour observed *via* measurements of the differences between the reduction and oxidation peak potentials (ΔE_p): 78 mV off-chip and 81 mV in the microfluidic device. Ideally, the ΔE_p for a reversible redox system such as ferrocyanide / ferricyanide redox couple should be 59 mV at 298K [27]. We attribute the slight deviation from ideal ΔE_p to a combination of: uncontrolled temperature, uncontrolled surface roughness and possible surface modification of the working electrode. Nevertheless, ΔE_p achieved here, is good in comparison to other microfluidic systems and is sufficient for our purposes.

We collected voltammograms from all 6 embedded working electrodes in the microchannel while subjected to flow rate Q_{TOT} = 1 $mL \cdot h^{-1}$ flow of 4 mM solution of $K_3Fe(CN)_6$. Peak positions were very uniform and could be normalized to account for difference in exposed electrode surface areas (data not shown). This opens the way for future studies that require position-dependent CV measurements. The next series of experiments were conducted on one electrode that was far away from the center of the channel in order that it would always be exposed to confinement flow stream (i.e. the red stream in figure 2C).

Fig. 5B shows the linear relationship between ferricyanide concentration and the redox peak currents as expected in a properly working system. We do not exploit concentration dependent measurements here, but such measurements can be beneficial in future applications. To demonstrate the systems' applicability to fast data acquisition we collected cyclic voltammograms were recorded for an 8 mM of potassium ferricyanide solution at increasing scan rates: 50 $mV \cdot s^{-1}$, 100 $mV \cdot s^{-1}$, 200 $mV \cdot s^{-1}$, 300 $mV \cdot s^{-1}$and 400 $mV \cdot s^{-1}$. Given the voltage range (approximately -300 to 200 mV)

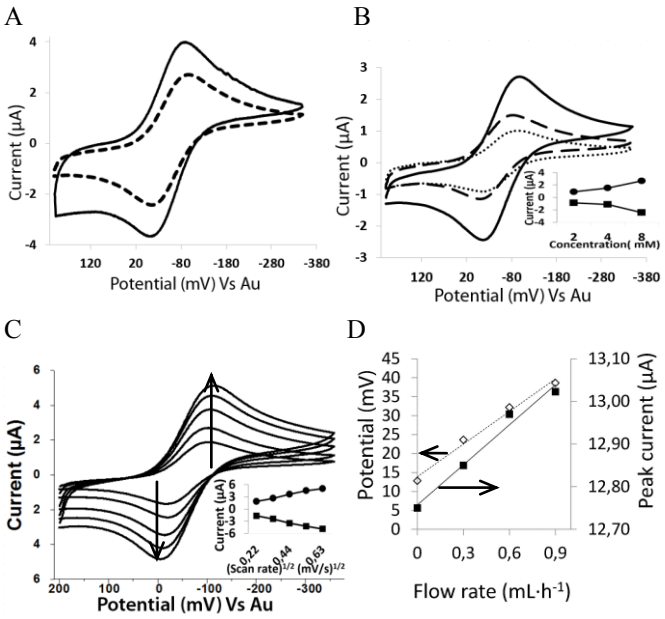

Fig. 5(A) Cyclic voltammogram of 6 mM aqueous potassium ferricyanide solution in bulk (solid) and microchannel (dashed) with scan rate of 100 $mV{\cdot}s^{-1}$. (B) Stacked cyclic voltammograms of potassium ferricyanide at 3 concentrations (2 mM, 4mM and 8mM) from an embedded working electrode within the microchannel. Inset shows trends in peak currents with concentration. (C) Stacked cyclic voltammograms of an 8 mM potassium ferricyanide solution at scan rates of 50 $mV{\cdot}s^{-1}$, 100 $mV{\cdot}s^{-1}$, 200 $mV{\cdot}s^{-1}$, 300 $mV{\cdot}s^{-1}$and 400 $mV{\cdot}s^{-1}$. Scan rates increase with the direction of the arrows. Inset shows trends in peak currents with $(\text{scan rate})^{1/2}$. (D) Shift in cathodic peak voltage (open) and current (solid) with liquid flow rate of a 4 mM potassium ferricyanide solution flowing at 0.3; 0.6 and 0.9 $mL{\cdot}h^{-1}$.

each complete voltammograms took between 20 s and 2.5s, depending on the scan rate. The peak intensities varied linearly with the square root of the scan rate as predicted by the Randles–Sevcik equation [28]. Finally, we measured the effect of flow rate on the current and potential of redox peaks. The changes to the cathodic peak current (μA) and position (mV) both vary linearly with flow rate (Fig. 5D) as expected, but the differences are not pronounced. It is known that sensitivity to flow velocity is enhanced for smaller electrodes, so it is planned to integrate smaller electrodes into the device for future applications which require higher sensitivity to the flow velocity.

IV. Results: Proof-of-Principle Measurements and Next Steps

A. Flow Templating Compartment

We tested the system components during template flow and biofilm growth. First, an inoculant stream flowed through Inlet 3 (Q_{TI} = 0.3$mL{\cdot}h^{-1}$) and emerged into the main measurement channel along with a co-flowing confinement stream from Inlet 1 (Q_C = 0.5 $mL{\cdot}h^{-1}$), i.e., Q_{TI}/Q_C = 0.6.

The inoculant stream flowed along the template wall where bacteria attached. After an inoculation time of 2 hours, the inoculant flow was stopped (Q_{TI} = 0 $mL{\cdot}h^{-1}$) and a pure citrate nutrient stream (no bacteria) was injected into Inlet 2 (Q_{TN} = 0.3 $mL{\cdot}h^{-1}$). Confinement results are discussed in Section IV.*C*.

B. SERS Characterization Compartment

In a separate experiment under similar flow conditions, we made Raman spectral imaging against a silver SERS surface to verify that we could monitor a citrate template solution confined to the center portion of the template wall with no external probe molecules or dyes (Fig. 6A). The silver SERS surface progressively lost its sensitivity with time of exposure to nutrient streams. Therefore, we are currently working to include and fully test a gold SERS surface into the SERS compartment, in order to increase its durability in the presence of microbes and strong salt concentrations.

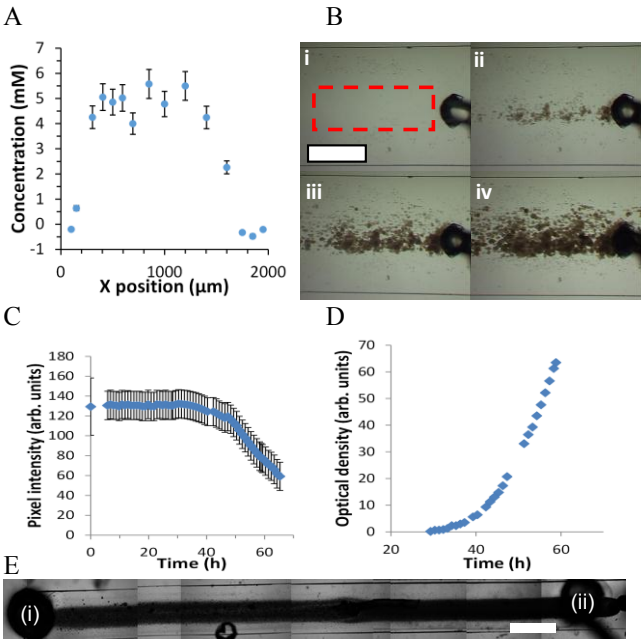

Fig. 6(A) SERS image of citrate concentration in the microchannel cross-section for 5 mM sodium citrate template stream and water confinement stream with flow rate ratio of Q_{TN}/Q_C = 0.45. (B) Time varying images of linear biofilm patterns during growth phase under flow rates Q_1 = 0.5$mL{\cdot}h^{-1}$ and Q_2=0.3$mL{\cdot}h^{-1}$. Images of template biofilms acquired in optical transmission mode at times, t_i=0, t_{ii}=40h, t_{iii}=50h, t_{iv}=55h. Flow rate ratio was Q_{TN}/Q_C = 0.6. Scale bar in (i) is 1 mm. (C) Average pixel intensity within the red box in (B)(i) for all image acquisition times. Error bars were acquired from the standard deviation in average pixel intensity in the images series shown in (B). (D) Calculated optical density from data shown in (C). (E) A linear biofilm cultured in the microfluidic device Q_1 = 0.3 $mL{\cdot}h^{-1}$, Q_2 = 1.0 $mL{\cdot}h^{-1}$. Image was acquired 50 h after inoculation.

C. Optical Characterization Compartment

During the exposure to nutrient flow, high resolution (100x magnification) microscope images of attached microbes were taken and their surface density in time could be counted using image analysis software (data not shown here). The low resolution (2x magnification) time series optical images in Fig. 6B showed the development of the biofilm during exposure to the templated citrate nutrient solution. The result was growth of biofilm downstream of the inoculant junction in time (Fig. 6A). No biofilm growth upstream of this location was observed initially, because there were no pre-adsorbed bacteria applied in these locations. The average pixel intensity and the standard deviation of the pixels in the region of the growing biofilm were determined by image analysis (Fig. 6C). Using a conversion described elsewhere

the optical density was determined, which is directly proportional to the biomass (Fig. 6D) [20]. Figure 6E shows the linear biofilm formation after 50 h of exposure to the templated nutrient solution.

D. Electrochemical Characterization Compartment

To determine the effect of the presence of the biofilm on the liquid flow velocity around it via CV, a redox active potassium ferrocyanide is added to the confinement stream. The electrode is localized to the portion of the channel containing only the confinement stream, thereby avoiding modifications to the electrode behaviour due to bacterial attachment. It also avoids direct contact of potassium ferrocyanide with the biofilm, though it is worth noting that this redox molecule is known to be nontoxic for gram-negative bacteria such as *Pseudomonas sp.* used in this work. Initial observations suggest that biofilm growth under the conditions after 60 h cultivation does not appreciably affect the flow velocity around it. Therefore, we preliminarily conclude that the biofilms were not growing appreciably in the direction perpendicular to the surface of the template wall or that they were porous enough to enable flow through, rather than around them. However, as discussed previously, the CV measurements' sensitivity to flow velocity is relatively low. Therefore, we plan to repeat these experiments using smaller, more sensitive electrodes [23]. Confocal laser scanning microscope data of biofilm height will also help to further validate the technique. Once fully implemented this will allow the comparison of sensitive real-time flow velocity measurements with optical and Raman measurements.

ACKNOWLEDGMENT

F.P.-M. acknowledges NSERC for postgraduate scholarship.

REFERENCES

[1] L. Hall-Stoodley, J. W. Costerton, and P. Stoodley, "Bacterial biofilms: From the natural environment to infectious diseases," *Nat. Rev. Microbiol.,* vol. 2, pp. 95-108, Feb 2004.
[2] M. Winn, J. M. Foulkes, S. Perni, M. J. H. Simmons, T. W. Overton, and R. J. M. Goss, "Biofilms and their engineered counterparts: A new generation of immobilised biocatalysts," *Catal. Sci. Technol.,* vol. 2, pp. 1544-1547, 2012.
[3] B. E. Logan, *Microbial fuel cells*. Hoboken, N.J: Wiley-Interscience, 2008.
[4] S. Haruta, T. Yoshida, Y. Aoi, K. Kaneko, and H. Futamata, "Challenges for Complex Microbial Ecosystems: Combination of Experimental Approaches with Mathematical Modeling," *Microbes Environ.,* vol. 28, pp. 285-294, Sep 2013.
[5] T. O. Peulen and K. J. Wilkinson, "Diffusion of Nanoparticles in a Biofilm," *Environ. Sci. Technol.,* vol. 45, pp. 3367-3373, Apr 2011.
[6] Y. Liu and J. H. Tay, "The essential role of hydrodynamic shear force in the formation of biofilm and granular sludge," *Water Res.,* vol. 36, pp. 1653-1665, Apr 2002.
[7] M. Salta, L. Capretto, D. Carugo, J. A. Wharton, and K. R. Stokes, "Life under flow: A novel microfluidic device for the assessment of anti-biofilm technologies," *Biomicrofluidics,* vol. 7, Nov 2013.
[8] J. H. Lee, J. B. Kaplan, and W. Y. Lee, "Microfluidic devices for studying growth and detachment of Staphylococcus epidermidis biofilms," *Biomed. Microdevices,* vol. 10, pp. 489-498, Aug 2008.
[9] L. Richter, C. Stepper, A. Mak, A. Reinthaler, R. Heer, M. Kast, H. Bruckl, and P. Ertl, "Development of a microfluidic biochip for online monitoring of fungal biofilm dynamics," *Lab Chip,* vol. 7, pp. 1723-1731, 2007.
[10] A. Valiei, A. Kumar, P. P. Mukherjee, Y. Liu, and T. Thundat, "A web of streamers: biofilm formation in a porous microfluidic device," *Lab Chip,* vol. 12, pp. 5133-5137, 2012.
[11] M. Skolimowski, M. W. Nielsen, J. Emneus, S. Molin, R. Taboryski, C. Sternberg, M. Dufva, and O. Geschke, "Microfluidic dissolved oxygen gradient generator biochip as a useful tool in bacterial biofilm studies," *Lab Chip,* vol. 10, pp. 2162-2169, 2010.
[12] H. J. Hou, L. Li, C. U. Ceylan, A. Haynes, J. Cope, H. H. Wilkinson, C. Erbay, P. de Figueiredo, and A. Han, "A microfluidic microbial fuel cell array that supports long-term multiplexed analyses of electricigens," *Lab Chip,* vol. 12, pp. 4151-4159, 2012.
[13] E. Bester, G. M. Wolfaardt, N. B. Aznaveh, and J. Greener, "Biofilms' Role in Planktonic Cell Proliferation," *Int. J. Mol. Sci.,* vol. 14, pp. 21965-21982, Nov 2013.
[14] J. S. L. Song, K. H. Au, K. T. Huynh, and A. I. Packman, "Biofilm Responses to Smooth Flow Fields and Chemical Gradients in Novel Microfluidic Flow Cells," *Biotechnol. Bioeng.,* vol. 111, pp. 597-607, Mar 2014.
[15] N. Babaei Aznaveh, M. Safdar, G. Wolfaardt, and J. Greener, "Micropatterned biofilm formations by laminar flow-templating," *Lab Chip,* to be published
[16] D. N. Hohne, J. G. Younger, and M. J. Solomon, "Flexible Microfluidic Device for Mechanical Property Characterization of Soft Viscoelastic Solids Such as Bacterial Biofilms," *Langmuir,* vol. 25, pp. 7743-7751, Jul 2009.
[17] F. Paquet-Mercier, N. B. Aznaveh, M. Safdar, and J. Greener, "A Microfluidic Bioreactor with in Situ SERS Imaging for the Study of Controlled Flow Patterns of Biofilm Precursor Materials," *Sensors,* vol. 13, pp. 14714-14727, Nov 2013.
[18] J. Kim, H. S. Kim, S. Han, J. Y. Lee, J. E. Oh, S. Chung, and H. D. Park, "Hydrodynamic effects on bacterial biofilm development in a microfluidic environment," *Lab Chip,* vol. 13, pp. 1846-1849, 2013.
[19] K. Drescher, Y. Shen, B. L. Bassler, and H. A. Stone, "Biofilm streamers cause catastrophic disruption of flow with consequences for environmental and medical systems," *Proc. Natl. Acad. Sci. U. S. A.,* vol. 110, pp. 4345-4350, Mar 2013.
[20] R. Bakke, R. Kommedal, and S. Kalvenes, "Quantification of biofilm accumulation by an optical approach," *J. Microbiol. Methods,* vol. 44, pp. 13-26, Feb 2001.
[21] Y. Chao and T. Zhang, "Surface-enhanced Raman scattering (SERS) revealing chemical variation during biofilm formation: from initial attachment to mature biofilm," *Anal. Bioanal. Chem.,* vol. 404, pp. 1465-1475, Sep 2012.
[22] J. C. Biffinger, J. Pietron, R. Ray, B. Little, and B. R. Ringeisen, "A biofilm enhanced miniature microbial fuel cell using Shewanella oneidensis DSP10 and oxygen reduction cathodes," *Biosensors & Bioelectronics,* vol. 22, pp. 1672-1679, Mar 2007.
[23] X. Illa, O. Ordeig, D. Snakenborg, A. Romano-Rodriguez, R. G. Compton, and J. P. Kutter, "A cyclo olefin polymer microfluidic chip with integrated gold microelectrodes for aqueous and non-aqueous electrochemistry," *Lab Chip,* vol. 10, pp. 1254-1261, 2010.
[24] M. Schlesinger, "Electroless and Electrodeposition of Silver," in *Modern Electroplating*, ed: John Wiley & Sons, Inc., 2010, pp. 131-138.
[25] H. J. Bai, M. L. Shao, H. L. Gou, J. J. Xu, and H. Y. Chen, "Patterned Au/Poly(dimethylsiloxane) Substrate Fabricated by Chemical Plating Coupled with Electrochemical Etching for Cell Patterning," *Langmuir,* vol. 25, pp. 10402-10407, Sep 2009.
[26] H. Zhang, J.-J. Xu, and H.-Y. Chen, "Shape-Controlled Gold Nanoarchitectures: Synthesis, Superhydrophobicity, and Electrocatalytic Properties," *J. Phys. Chem. C,* vol. 112, pp. 13886-13892, Sep 2008.
[27] S. Eisele, M. Schwarz, B. Speiser, and C. Tittel, "Diffusion coefficient of ferrocene in 1-butyl-3-methylimidazolium tetrafluoroborate - concentration dependence and solvent purity," *Electrochim. Acta,* vol. 51, pp. 5304-5306, Jul 2006.
[28] N. S. Neghmouche and T. Lanez, "Electrochemical properties of N'-ferrocenylmethyl-N'-phenylbenzohydrazide in aqueous and organic mediums " *Int. Lett. Chem., Phys. Astron.,* vol. 5, pp. 76-85, 2013.